https://doi.org/10.20575/00000047
Polar Data Journal, Vol. 7, 35–49, July 2023

Long-term all-sky-camera images and evaluated cloud-cover data at Syowa Station, Antarctica

Naohiko HIRASAWA[1,2]*, Masanori YABUKI[3], Masataka SHIOBARA[1,2]**, Yumi SHIMODE[4] and Makoto KUJI[5]

[1] National Institute of Polar Research, Research Organization of Information and Systems, 10-3, Midori-cho, Tachikawa, Tokyo 190-8518.

[2] Department of Polar Science, School of Multidisciplinary Sciences, SOKENDAI (The Graduate University for Advanced Studies), 10-3, Midori-cho, Tachikawa, Tokyo 190-8518.

[3] Research Institute for Sustainable Humanosphere, Kyoto University, Gokasho, Uji, Kyoto 611-0011.

[4] Graduate School of Humanities and Sciences, Nara Women's University, Kitauoyanishi-machi, Nara 630-8506.

[5] Division of Natural Sciences, Faculty, Nara Women's University, Kitauoyanishi-machi, Nara 630-8506.

*Corresponding author. Naohiko Hirasawa (hira.n@nipr.ac.jp)

**Currently retired

(Received September 8, 2022; Accepted June 16, 2023)

Abstract: We acquired fish-eye camera (referred to as all-sky-camera) images for detection of cloud distribution in the entire sky and also for use as reference data for optical observations (i.e., sky radiometry[1] and micro-pulse lidar[2,3] observations) conducted at Syowa Station (69°00′S, 39°35′E), Antarctica, from 2006 to 2022 as a part of a scientific project entitled, “Monitoring observations of the Antarctic aerosols and clouds” as part of the Japanese Antarctic Research Expedition (JARE) program. We evaluated the cloud cover in all the images captured over this period using an objective algorithm based on the brightness of the RGB colors of the images. The importance of cloud properties in climate change models is well known, and obtaining long-term information on cloud properties is important for atmospheric monitoring over Antarctica. This paper describes the archives of all-sky-camera images, evaluated cloud-cover images, and text data of time series of evaluated cloud amounts for this period. Compared with eye observation, the evaluated cloud amounts from the all-sky-camera are underestimated by about 10%. Still, the so-called “U-shaped” frequency distribution is common, where the frequency increases near the maximum and minimum cloud amounts. In addition, we briefly touch on the method of cloud detection. The data are available from the National Institute of Polar Research (NIPR) at https://scidbase.nipr.ac.jp/modules/metadata/index.php?content_id=138.

1. Background and Summary

In global warming studies, the role of polar amplification on warming rates has been observed and demonstrated by most predictive models[4]. Among the many climate feedback systems that have been investigated to date, aerosol-cloud-radiation processes are the most complicated. Indeed, in many cases, the extent to which multiple effects of the processes will have a positive or negative effect on global warming is not yet fully known with certainty[5]. As a result, long-term monitoring of aerosol-cloud-radiation processes is considered important for accurately predicting future changes in climate.

In response to the need for such long-term observations, a project titled "Monitoring observations of the Antarctic aerosols and clouds" was launched by the Japanese Antarctic Research Expedition (JARE) to record atmospheric properties related to radiation processes at Syowa Station (69°00′ S, 39°35′ E). The primary instruments used in the project include micro-pulse lidars[6,7,8,9] to acquire the vertical distribution of optical scatterers and a sky-radiometer[10] to estimate the properties of these scatterers in radiation processes. As optical scatterers are composed mainly of aerosols and cloud particles, observations involve both mixed aerosol and cloud effects. To isolate the effect of clouds on observations, we have implemented all-sky photography using an all-sky-camera system from 2006 to 2022.

We have already started distributing the all-sky-camera images through the Arctic and Antarctic Data archive System (AADS)[11]. We further evaluated cloud cover based on the images throughout the entire data collection period using an algorithm developed by Yabuki *et al.* (2014)[12], who confirmed the validity of the algorithm for cloud cover detection at Ny-Ålesund, Norway. Since the impacts of cloud dynamics on global warming and the climate of any part of the globe are complicated, continuous monitoring observations are considered necessary. Therefore, we evaluate long-term fluctuations in cloud cover above Syowa Station and publish these findings here together with the all-sky-camera images. This paper describes the newly prepared archives of the all-sky-camera images, evaluated cloud-cover images, and text data of time series of evaluated cloud amount and summarizes the evaluated cloud cover data.

2. Location and duration of observations

Figure 1a shows a map of Antarctica and the location of Syowa Station (69°00′ S, 39°35′ E). The all-sky-camera system was installed on the roof of an atmospheric observatory at Syowa Station (Fig. 1b).

The observations started on 18 January 2006 and ended on 1 December 2022, when the parent project will be terminated. As shown in Table 1, data were not captured on several occasions due to trouble with equipment or to avoid damage due to low temperatures during the polar night.

Data processing of cloud cover was performed from 10 August to 30 April when there was sufficient light in the daytime for cloud detection in the images.

We publish all of the image data from 18 January 2006 to 1 December 2022 and the cloud detection data from 18 January 2006 to 10 January 2020 through an URL, as described in Section 4. We decided not to perform cloud evaluation on the data after 10 January 2020 because the quality of the data is no longer sufficient for the evaluation due to aging of the instruments.

3. Instrument and methods

The all-sky-camera system (PSV-100, Prede Co. Ltd., Japan) is shown in Fig. 1b. The system has been installed on the roof of an atmospheric observatory at Syowa Station. The same series of systems have been replaced twice with a spare system on 20 December 2009 and on 11 January 2020. The camera is inside a windbreak and cold protection device equipped with a sun tracking shield (hereafter referred to as a sun-shield), which excludes sunlight from the images (Fig.2a). The digital images are in jpeg format and recorded using RGB colors. The shooting interval is usually 10 minutes, with 5 or 2 minutes intervals for short partial periods.

We evaluated the cloud cover for each of the images using the algorithm of Yabuki *et al.*[12]. We first selected several clear-sky images with different sun elevations from August to April for individual summer seasons. Second, using the selected clear sky images for the individual summers, we constructed a unique clear sky reference table showing the intensities of R, G, and B, as well as several sun elevation angles. Finally, we performed a supervised classification of each pixel in an image into cloud-free and cloud pixels. The algorithm evaluates the anomalous brightness of the pixels from the clear sky reference table to judge the appearance of clouds. In Yabuki's algorithm, optically thick clouds or very bright clouds are first extracted as type A clouds. The very bright clouds include some optically thin clouds. Optically thin, less bright clouds in the rest of the area are extracted as type B. These type B clouds are evaluated by their spectral contrast between the RGB components and the spatial variability of the brightness. However, note that type A and type B are just clouds detected by two methods based on the characteristics of the brightness distribution of the image, and do not represent characteristics quantitatively such as optical depth of clouds. Therefore, this algorithm finally combines type A and type B clouds to identify cloud areas and cloud amounts. Figure 2 shows examples of all-sky-camera images and the detected cloud distribution. We will discuss the issues involved in this cloud detection result in section 5.

4. Data Records

Here we describe the directory structure for the data archive. The parent directory of the ftp site is “asc”. Under the “asc” parent directory, there are seventeen directories for each year (e.g., “2006”, … “2022”, etc.) and within these directories are subdirectories for each day containing the jpeg-

formatted image data. The name format used for the daily directories is, for example, “20080101” for 1 January 2008. We also archived files compressed by the zip command for each directory of the year.

The “cloud” directory in the “asc” parent directory contains the files generated by applying the cloud detection algorithm. The cloud distribution images, e.g., Figs. 2b and d, are recorded in png format and are archived in a daily subdirectory under the yearly directory. We also archived files compressed by the zip command for each directory of the year.

We recorded the results of cloud evaluation in plain text files. For example, the file name for 10 August 2020 to 30 April 2021 is “Syowa-cloud-2020-2021.txt”. The data were recorded on one line for each image at 10-minute intervals. The order of the data is as follows: date (yyyy/mm/dd), time (hh:mm:ss), sun zenith angle (degrees), sun azimuth (degrees), cloudless pixel ratio (%), type-A-cloud pixel ratio (%), type-B-cloud pixel ratio (%), effective pixel count (N), the number of insufficient brightness pixels (N). The three ratios above are obtained by dividing them by the effective pixel count. The summation of the effective pixels and the insufficient brightness pixels is 112558, which are the pixels used in the analysis. If the ratio of insufficient brightness pixels to 112558 is more than 20%, we did not apply the cloud analysis (no records of cloud).

A supplemental file “data-information_v20220906.txt” under the directory of “asc/cloud/” records information related to the uncertainty of the data. The file name reflects the data the information was last updated. We will discuss those and the record format in the file in section 5. Moreover, we will continue adding information to this file in the future according to new findings, which will be performed according to the version control of the data publication regulations.

5. Technical validation

5.1. Cloud detection

In general, cloud cover observations are still carried out by meteorological observers performing eye observations. Given the subjective nature of such observations, different observers may record their observations differently, even for the same sky. Since the method for cloud cover evaluation described in this study is based on objective procedures with digital data, the obtained results are generally consistent for the same sky. However, even with this objective evaluation method, the results obtained for the same sky can vary.

There are four major possible explanations for fluctuations in the evaluation results. One is due to differences in the set of clear-sky images used as reference images. To control this possibility, images acquired at various solar zenith angles are included in the set. The second reason is that the intensities of each of the three primary colors, R, G, and B, are lower than the original value at the time of manufacture due to the deterioration of the camera sensor over time. To control this possibility, the clear-sky images were reselected each year to create a set of reference images that

reflected the deterioration over time. The third reason is due to changes in the surface albedo. In polar regions, cloud detection using camera images usually suffers from uncertainties in fractional cloud cover retrieval because of the inhomogeneity of the sky radiance distribution reflected by the high surface albedo at large zenith angles (near the horizon). Therefore, we decided the target area of the images within 70 degrees of zenith angle (larger than 20 degrees of elevation angle). The annual update of the reference images for various solar zenith angles also reduces the uncertainty associated with the surface albedo. The final reason is that the brightness of the image can change randomly. The cause of this is unknown, but this is a low-temperature environment, and the working of the camera may become less stable. Since it is not possible to fully account for this factor, we decided to exclude those with dark images as a whole from the cloud analysis. By this operation, the images at solar zenith angles larger than 85 degrees (solar elevation angles lower than 5 degrees) are automatically excluded from the analysis target. However, the evaluated cloud cover data may still include the effects of such fluctuations in brightness.

Figure 2 shows examples of the all-sky-camera images (on the left-hand side of the figure) and the evaluated cloud distribution (on the right-hand side). A black rectangular in each all-sky-camera image is the sun-shield, and another rectangular in each evaluated cloud distribution is the area that is set to overlap over the sun-shield and the vicinity area and is excluded from the cloud detection. In the first set of examples (Figs.2a and b), the clear sky area and cloud distribution are generally judged correctly. However, in the all-sky-camera image, we can find thin clouds spreading around the label "Thin", but the cloud analysis determined that most of the area is clear sky. Therefore, the threshold used in this algorithm is not appropriate for this thin cloud. However, another threshold may identify a cloudless sky as a cloud, as discussed below.

Yabuki *et al.*[12] demonstrated the validation of the cloud detection algorithm using the 2086 hourly all-sky-camera images and the collocated micro-pulse lidar data in May for the years 2005–2007 at the Arctic Ny-Ålesund Station. The micro-pulse lidar, which is an active remote sensing system, can detect very optically thin clouds compared with the all-sky-camera image analysis. When no clouds were detected by the micro-pulse lidar, the false cloud detection rate from all-sky-camera image analysis classification was 2.1% in total hours. Conversely, when clouds were detected by the micro-pulse lidar, the all-sky-camera image analysis classification underestimated 11.6% of the clouds in the image. The vicinity of the label "Thin" would be an example of this.

Figures 2c and d include multiple problems. First, the miss-controlled sun-shield (the label A in Fig. 2c) could not cover the sun (the label B in Fig. 2c). As a result, the sun-shield created another black area (the label A in Fig. 2d) apart from the black area of the analysis exclusion, (the label A’ in Fig. 2d). Pixel counts of the sun-shield were about 5250, which is about 5% of the analyzed area. This effect reflects the number of insufficient brightness pixels recorded in the plain text file. Second, the analysis exclusion area (the label A’ in Fig. 2d) also did not overlap the sun (the label B in Fig. 2d). A false cloud area was detected there. The analysis exclusion area is set in the algorithm

according to the time of the image. The reason for this trouble would come from either of incorrect time stamp or an incorrect azimuth angle of the instrument. We recorded the occurrence of this trouble in a supplemental file using the word of "TFSS" (Tracking failure of the sun-shield plate). The supplement file is in the directory of "asc/cloud" and the name is "Supplement_information.txt".

Third, we find another false cloud area (the label C in both Figs. 2c and d), which is caused by multiple reflections of sunlight on the glass dome. Such cases often occurred at relatively low elevation angles of the sun. However, it is difficult to determine this area automatically. Since false cloud areas were not large as 2.96% for type-A and 2.32% for type-B in this case, we did not correct the overestimation due to the manifestation of these phenomena in this analysis. Therefore, note that in the text data files such as "Syowa-cloud-2020-2021.txt", some cases with cloud amount less than 5% include clear skies (completely cloudless).

Figures 2e and f show a case when frost had grown on the sun-shield. Our analysis judged the frost area as a type-A cloud. We recorded the occurrence of such frost on the sun-shield in the supplemental file using the word of "FRST" (FRST: Frost on the sun-shield plate).

Figures 2g and h show a case where precipitation droplets adhere to the glass dome. We find that the droplets were on the entire area of the glass dome in Fig. 2g though there were areas that were difficult to see due to the effect of light scattering. Our analysis judged some parts of the droplet areas as clear sky portions or type-B clouds with the background of type-A clouds. We recorded the occurrence of such case in the supplemental file using the word of "PD" (PD: Precipitation droplet on the glass dome).

We touch the data format of the supplemental file ("Suplement_information.txt"). The main body consists of an each date or period list for every year, which is divided a line written such as "2. 2006.08-2007.04" for a period of 10 August 2006 to 30 April 2007. Supplemental information is given following each date or period. As the supplemental information, the following three terms are provided: TFSS (Tracking failure of the sun-shield plate), PD (Precipitation droplet on the glass dome), and FRST (Frost on the sun-shield plate). The order of the information in a line is as follows: year, month, date, and terms or year, month, date, "-", month, date, and terms. The latter case means a period. In the future, as research progresses, we may revise the supplemental file if we notice new information worth recording.

5.2. Aging deterioration of the all-sky-camera system

In the all-sky-camera images after August 2019, the troubles of the sun-shield control had frequently occurred. The damages of the images lead to increase dark pixels of the sun-shield that were excluded in the cloud detection process. Then, on 11 January 2020, we replaced it with a spare system that the aging was same as the previous system. The spare system controlled the sun-shield but the quality of the images have been low. Double images (Fig.3a) and fine misalignment (Fig.3b) frequently occurred. These effects became even stronger after August 2020. These damages of the

images lead to increase false clouds that decrease accuracy of this data-set in addition to the increase in dark pixels. Figure 4 shows time series of monthly mean of the number of dark pixels from August 2018 to April 2022. The monthly mean numbers of the dark pixels were very few until April 2019 but they increased suddenly in August 2019 and increased even more in August 2021. In August 2019, the sunshield got not to work properly. The sunshield, which is located at a different position from the sun, creates extra dark pixels. This dark pixel area was at most 5% of the whole analysis area. When we detected clouds from these images with the current algorithm, the number of false clouds increased after 11 January 2020, when the system was replaced with a spare system (not shown here). Therefore, we have decided to perform the cloud evaluation for the period up to 11 January 2020.

5.3. Comparison with eye observation at Syowa Station

Finally, we validate this cloud detection on the all-sky-camera images with a comparison with eye observation conducted by the Japan Meteorological Agency. Figure 5 is a comparison of monthly cloud amounts between the all-sky-camera estimation with a 10-minute interval and the eye observation with a 3-hour interval. The cloud amounts are most abundant in the range of 60% to 90% with a roughly linear relationship. The plot with label “A” is for January 2012. The larger differences of the all-sky-camera estimation from the eye observations is due to the short periods of the all-sky-camera images for three days, January 29–31. Overall, however, we find that the all-sky-camera estimation is about 10% underestimated compared to the eye observation. Indeed, the standard deviation of those differences is 11.5% over the entire period (February 2006–January 2020). This underestimation is consistent with those of Yabuki *et al.*[12] using Arctic data. However, the monthly mean time variability characteristics are generally consistent between the all-sky-camera estimation and eye observation (Fig. 6).

Table 2 shows a simultaneous comparison between eye observation (EYE) and all-sky-camera estimation (ASC) from 10 August 2006 to 30 April 2007. In all, 1011 cases were matched. A common feature shared by eye observations and the all-sky-camera estimation is the higher frequency of occurrence by cloud amount at 10 in eye observation (100% in the all-sky-camera estimation) and 0 (same, 0%). This U-shaped frequency distribution[13] holds when using the all-sky-camera data every 10 minutes (Fig.7). The U-shaped frequency distribution was observed at Mizuho Station inland Antarctica[14]. Table 2 shows how the all-sky-camera estimation underestimates in each time shot partially appears. For example, the all-sky-camera estimates the cloud amount to be less than 90% when the eye observation shows a cloud amount of 10, and in some cases, the cloud amount is 0%. The tendency of underestimation in the all-sky-camera estimation is more obvious in cases where the cloud amount in the eye observation is less than 10. This is because the all-sky-camera estimation does not detect thin clouds (Fig.2a); we may see that the all-sky-camera estimation detects clouds more effective in radiative processes.

6. Figures

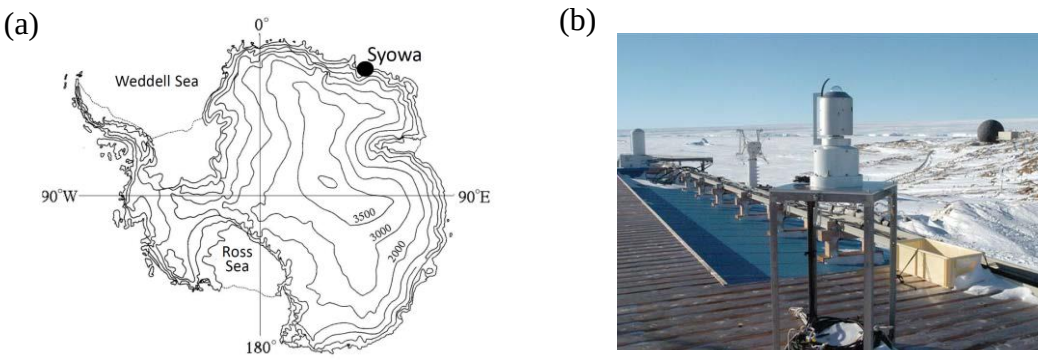

Figure 1. (a) Map of Antarctica showing Syowa Station. (b) The all-sky-camera system on the roof of an atmospheric observatory at Syowa Station. The camera is installed inside a windbreak and cold protection device equipped with a sun tracking shield.

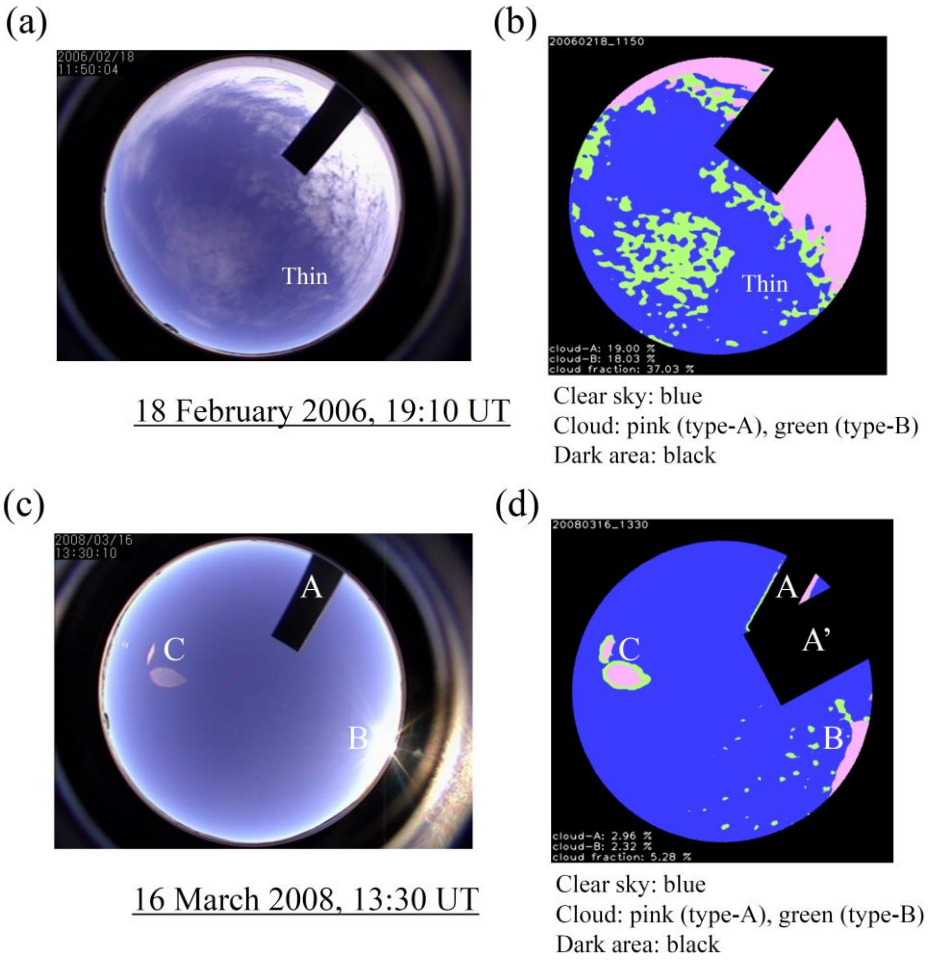

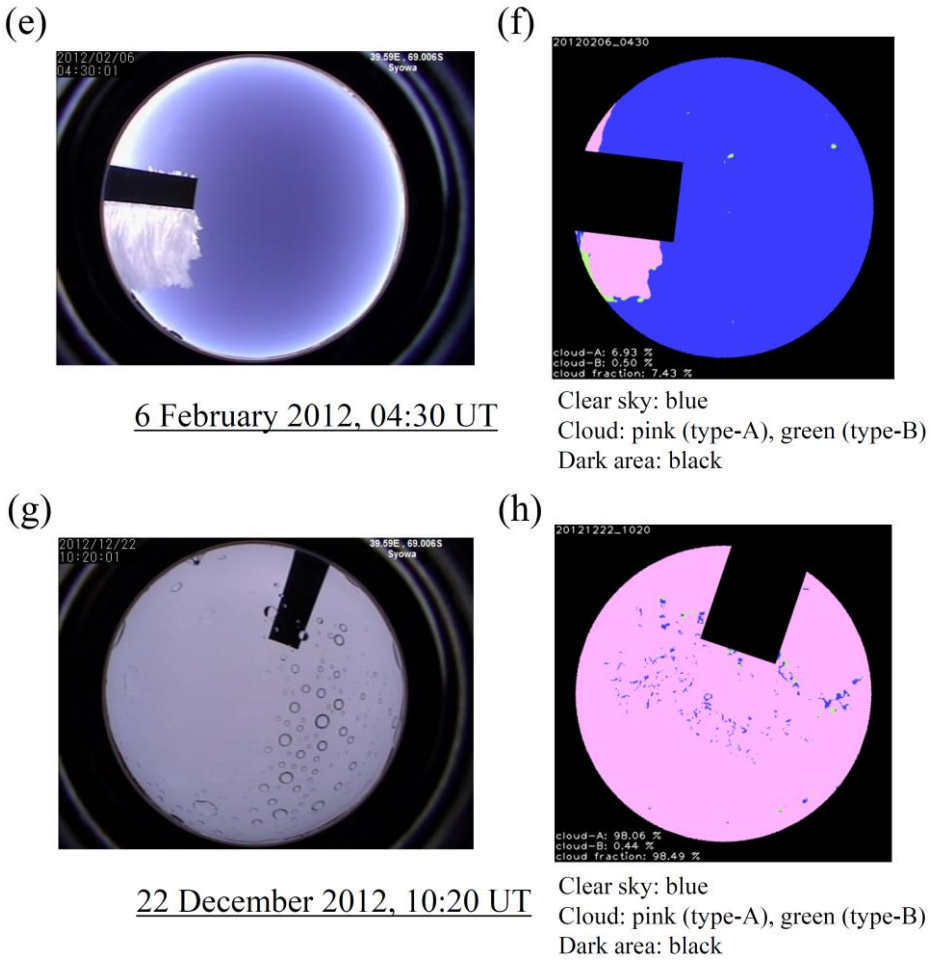

Figure 2. Demonstration of cloud detection and troubles and natural phenomena affecting detection. RGB color images on the left-hand side and results of cloud estimation on the right-hand side. (a)–(b) An example of a general result of cloud detection, focusing on the detection of thin cloud areas on 18 February 2006, at 11:50 universal time (UT). (c)–(d) An example where the sun-shield (A) and analysis exclusion area (A') did not overlap the sun, resulting in detection of a false cloud area around the sun (B) on 16 March 2008, at 13:30 UT. False cloud areas (C) due to multiple reflections of sunlight are also exemplified. (e)–(f) An example of images with frost on the sun-shield on 6 February 2012, at 04:30 UT. (g)–(h) An example of images with precipitation droplets on the glass dome on 22 December 2012, at 10:20 UT.

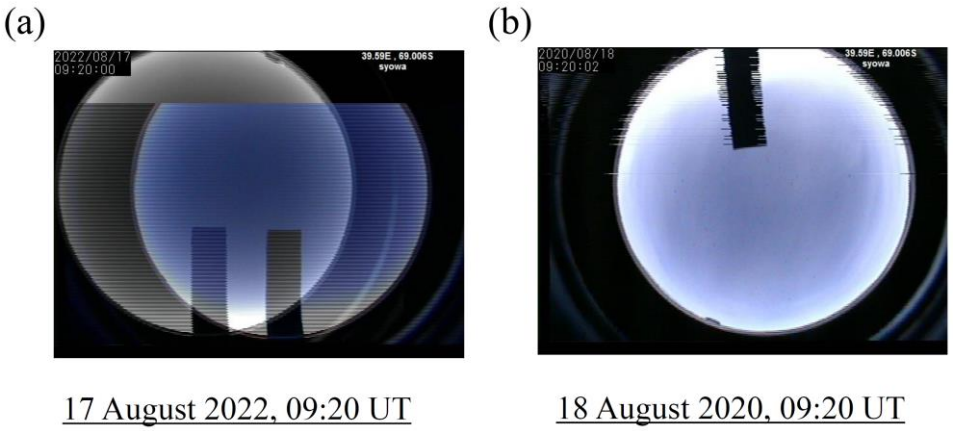

Figure 3. Examples of the troubles in quality of the all-sky-camera images after 11 January 2020. (a) Double images. (b) Fine misalignment.

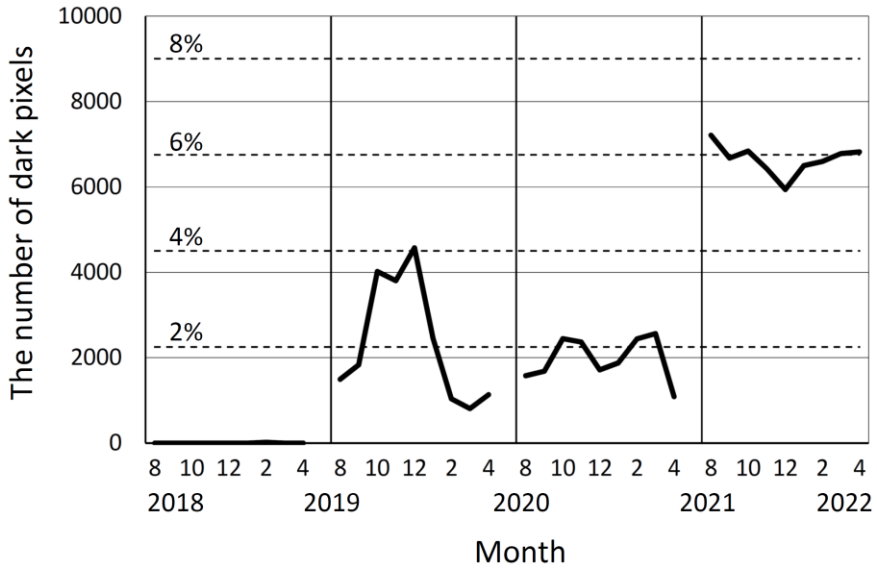

Figure 4. Time series of monthly mean of the number of dark pixels from August 2018 to April 2022. The horizontal dashed line indicates the ratio (%) of the number of dark pixels to the number of fully analyzed pixels (112558).

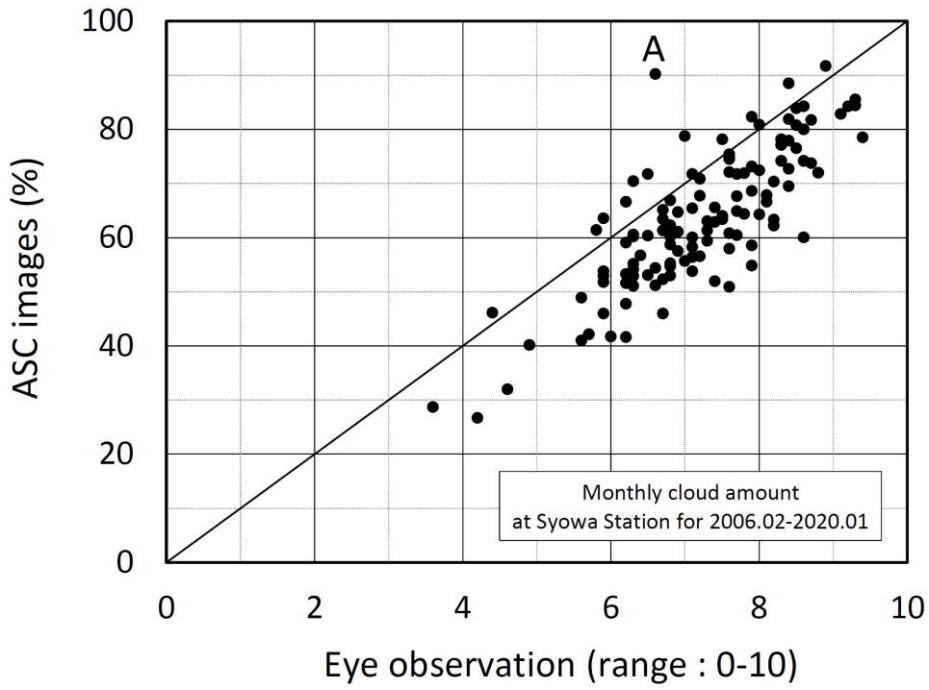

Figure 5. Comparison of monthly cloud amounts between this estimation derived from the all-sky camera (ASC) images and eye observation conducted by the Japan Meteorological Agency (JMA). The plot with label “A” is for three days from 29 to 31 January 2012.

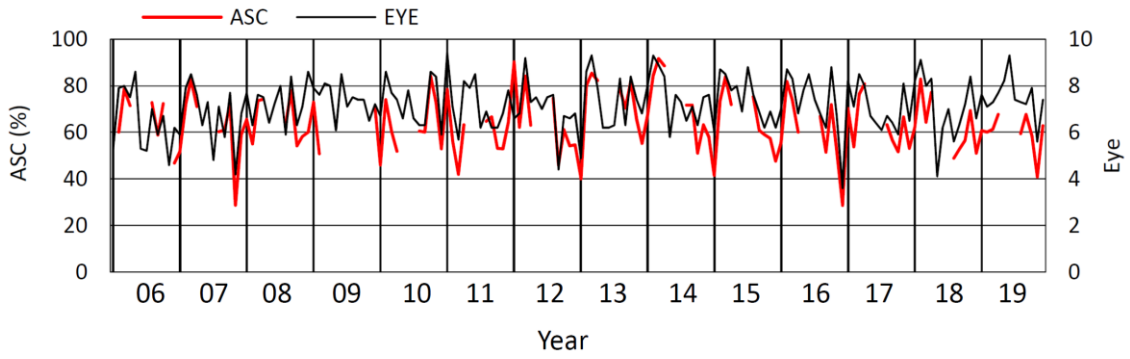

Figure 6. Time series of monthly cloud amounts of the all-sky-camera (ASC) estimation and eye observation.

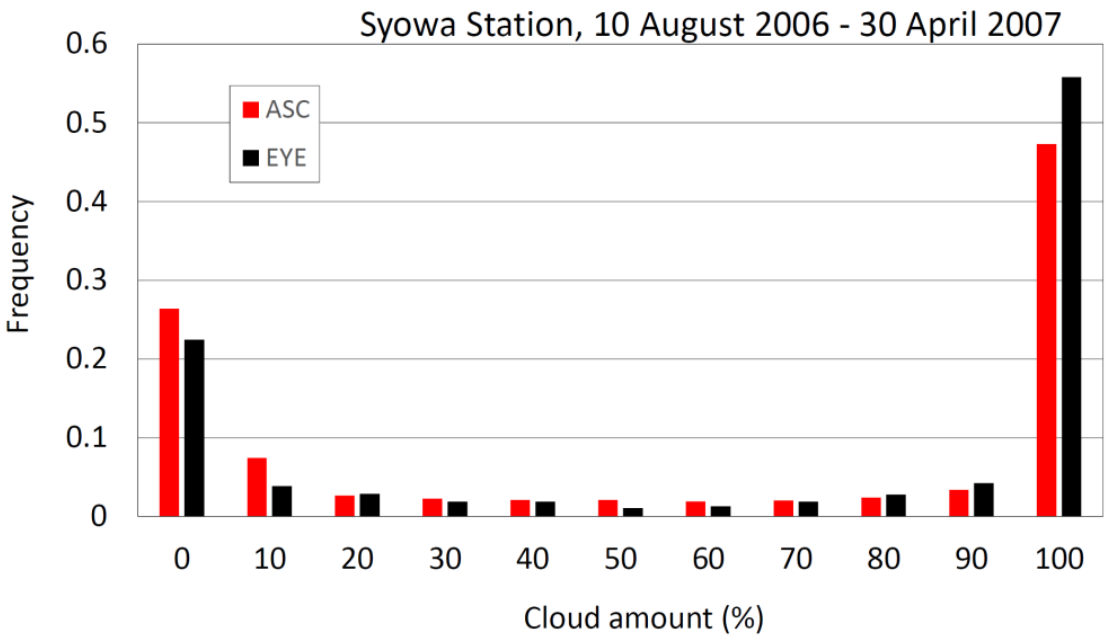

Figure 7. Frequency of occurrence for each cloud amount range for eye observations (EYE) with a 3-hour interval and all-sky-camera analysis (ASC) with a 10-minute interval for the period from 10 August 2006 to 30 April 2007. Eye observations are expressed as a scale of 0 to 10 with 0% to 100%. For all-sky-camera analysis, less than 5% is expressed as 0% range and between 5% and 15% as 10% range. The frequencies of occurrence are expressed with 0 to 1.

7. Table

Table 1. Major periods with no data of the all-sky-camera.

Major periods of no data	Reason
11 October - 14 December 2006	Equipment failure (hourly data record)
21 February - 19 December 2009	Equipment failure
10 June - 3 July 2010	Polar night
9 June - 5 July 2011	Polar night
1 January - 27 January 2012	Equipment failure
1 June - 12 July 2017	Polar night
19 May - 31 July 2018	Polar night
1 June - 12 July 2019	Polar night
20 May - 29 July 2020	Polar night
7 June - 2 August 2021	Polar night
11 May - 14 August 2022	Polar night

Table 2. Simultaneous comparison between eye observation (EYE) and all-sky-camera analysis (ASC) for the period from 10 August 2006 to 30 April 2007. The expression for the all-sky-camera is the same as in Fig.6.

ASC (%) / Eye	Total	0	10	20	30	40	50	60	70	80	90	100
0	227	205	21	0	0	0	1	0	0	0	0	0
1	39	34	5	0	0	0	0	0	0	0	0	0
2	29	18	10	1	0	0	0	0	0	0	0	0
3	19	11	7	1	0	0	0	0	0	0	0	0
4	19	7	7	2	1	1	0	1	0	0	0	0
5	11	3	6	1	0	0	0	1	0	0	0	0
6	13	2	5	3	2	0	0	1	0	0	0	0
7	19	2	10	2	0	1	0	1	2	1	0	0
8	28	2	7	7	3	0	2	1	0	1	2	3
9	43	3	6	3	4	0	2	1	4	4	4	12
10	564	6	9	17	19	12	13	11	17	20	27	413

Author contributions

Naohiko Hirasawa processed all the data and was the lead in writing this manuscript. Masanori Yabuki coded the program used to estimate the amount of cloud cover in the all-sky-camera images. Masataka Shiobara designed and organized most of this study and selected the instrument. Yumi Shimode and Makoto Kuji were partly responsible for processing cloud cover data and evaluated the result.

Acknowledgements

This study was conducted as a part of a scientific project entitled “Monitoring observations of the Antarctic aerosols and clouds,” performed as part of the Japanese Antarctic Research Expedition (JARE) program. The authors would like to express their deep gratitude to the members who performed observations and maintained the observation equipment at Syowa Station from 2006 to 2022.

References

1. SKYNET. Research Product Release Service at Center for Environmental Remote Sensing (CEReS). Chiba University. http://atmos3.cr.chiba-u.jp/skynet/data.html (accessed 2023-6-30).
2. Masanori Yabuki and Naohiko Hirasawa. Antarctic Micro-pulse lidar measurement (Antarctic MPL). Kyoto University and National Institute of Polar Research. https://scidbase.nipr.ac.jp/modules/metadata/index.php?content_id=140 (accessed 2023-6-30).
3. Masanori Yabuki and Naohiko Hirasawa. Antarctic Polarization Micro-pulse lidar measurement (Antarctic PMPL). Kyoto University and National Institute of Polar Research. https://scidbase.nipr.ac.jp/modules/metadata/index.php?content_id=398 (accessed 2023-6-30).
4. IPCC, 2021. Climate Change 2021: The Physical Science Basis. Contribution of Working Group I to the Sixth Assessment Report of the Intergovernmental Panel on Climate Change [Masson-Delmotte, V. et al. (Eds.)]. Cambridge University Press. 2021, 2391 p. https://www.ipcc.ch/report/sixth-assessment-report-working-group-i/ (accessed 2023-6-30).
5. Szopa, S. et al. “Short-Lived Climate Forcers”. Climate Change 2021: The Physical Science Basis. Contribution of Working Group I to the Sixth Assessment Report of the Intergovernmental Panel on Climate Change [Masson-Delmotte, V. et al. (Eds.)]. Cambridge University Press. 2021, p. 817–921.
6. Shiobara, M., Yabuki, M., and Kobayashi, H. A polar cloud analysis based on Micro-pulse Lidar measurements at Ny-Alesund, Svalbard and Syowa, Antarctica. Physics and Chemistry of the Earth. 2003, 28, p. 1205–1212. https://doi.org/10.1016/j.pce.2003.08.057.
7. Shibata, T., Sato, K., Kobayashi, H., Yabuki, M., and Shiobara, M. Antarctic polar stratospheric clouds under temperature perturbation by nonorographic inertia gravity waves observed by micro pulse lidar at Syowa station. J. Geophys. Res. 2003, 108 (D3), 4105. https://doi.org/10.1029/2002JD002713.
8. Hara, K. et al. Haze episodes at Syowa Station, coastal Antarctica: Where did they come from? J. Geophys. Res. 2010, 115, D14205. https://doi.org/10.1029/2009JD012582.
9. Kuji, M., Miyagawa, M., and Shiobara, M. Cloud features observed at Syowa Station. Antarctic ice sheet, atmosphere, aerosols, and climate [Hirasawa, N. and Yamanouchi, T. (eds.)], Kishou Kenkyuu Note. 2017, 233, p. 345–354. (in Japanese)
10. Kobayashi, H., Tanaka, N., and Shiobara, M. Long-term variations in the optical thickness and the optical properties of aerosols observed by a sky-radiometer at Syowa Station. Antarctic ice sheet, atmosphere, aerosols, and climate [Hirasawa, N. and Yamanouchi, T. (eds.)], Kishou Kenkyuu Note. 2017, 233, p. 355–362. (in Japanese)
11. VISHOP. Arctic and Antarctic Data archive System. International Polar and Earth Environmental Research Center (IPERC), National Institute of Polar Research (NIPR) , and Research Organization of Information and Systems (ROIS) . https://ads.nipr.ac.jp/vishop/#/monitor/type=mpl&site=Syowa&product=IMAGE (accessed 2023-07-03).

12. Yabuki, M., Shiobara, M., Nishinaka, K., and Kuji, M. Development of a cloud detection method from whole-sky color images. Polar Science. 2014, 8(4), p. 315–326. https://doi.org/10.1016/j.polar.2014.07.004.
13. Henderson-Sellers, A., Hughes, N. A., and Wilson, M. Cloud Cover Archiving on a Global Scale: A Discussion of Principles. Bulletin of the American Meteorological Society. 1981, 62(9), p. 1300–1307. https://doi.org/10.1175/1520-0477(1981)062<1300:CCAOAG>2.0.CO;2.
14. Yamanouchi T. A simple cloud-radiation statistics at Mizuho Station, Antarctica. Mem. Natl. Inst. Pol. Res. Special issue, 1985, 39, p. 87–96.

Data Citations

Hirasawa, N., Yabuki, M., Shiobara, M., Shimode, Y., and Kuji, M. (2023): Long-term all-sky-camera images and evaluated cloud cover data at Syowa Station, Antarctica. Pol. Data Jour., 7, 35–49. https://doi.org/10.17592/002.2023060138.